Shallow water acoustic channel estimation using two-dimensional frequency characterization

Naushad Ansari,[1,a)] Anubha Gupta,[1] and Ananya Sen Gupta[2]
[1]*Signal Processing and Bio-medical Imaging Lab (SBILab), Department of Electronics and Communication Engineering, Indraprastha Institute of Information Technology, Delhi, India*
[2]*Department of Electronics and Communication Engineering, University of Iowa, Iowa City, Iowa 52242, USA*

(Received 25 April 2016; revised 16 September 2016; accepted 28 October 2016; published online 28 November 2016)

Shallow water acoustic channel estimation techniques are presented at the intersection of time, frequency, and sparsity. Specifically, a mathematical framework is introduced that translates the problem of channel estimation to non-uniform sparse channel recovery in two-dimensional frequency domain. This representation facilitates disambiguation of slowly varying channel components against high-energy transients, which occupy different frequency ranges and also exhibit significantly different sparsity along their local distribution. This useful feature is exploited to perform non-uniform sampling across different frequency ranges, with compressive sampling across higher Doppler frequencies and close to full-rate sampling at lower Doppler frequencies, to recover both slowly varying and rapidly fluctuating channel components at high precision. Extensive numerical experiments are performed to measure relative performance of the proposed channel estimation technique using non-uniform compressive sampling against traditional compressive sampling techniques as well as sparsity-constrained least squares across a range of observation window lengths, ambient noise levels, and sampling ratios. Numerical experiments are based on channel estimates from the SPACE08 experiment as well as on a recently developed channel simulator tested against several field trials.
[http://dx.doi.org/10.1121/1.4967448]

[JFL] Pages: 3995–4009

I. INTRODUCTION

Undersea communications and related signal processing techniques have been richly investigated over the last few decades.[1–9] Despite phenomenal advancements in underwater acoustic (UWA) propagation models and related channel representations,[9,10] tracking the UWA channel in shallow water depths in real time is still an active challenging problem.

While several complementary approaches have been suggested toward shallow water acoustic channel estimation,[1–9] the fundamental challenges to real-time channel tracking remain a bottleneck. Specifically, these challenges are posed by two well-known properties of the shallow water acoustic channel:

(1) Long time-varying delay spread of the shallow water acoustic channel due to primary and secondary multipath reflections from the moving ocean surface and static sea bottom;[11] and
(2) Unpredictable high-energy transients in the UWA channel delay spread due to oceanographic events such as caustics and other forms of ephemeral oceanic events such as surface wave focusing.[12] This adds another layer of challenge by leading to non-stationarity in the underlying channel distribution.[1]

These challenges are discussed in more detail below in the context of different types of multipath arrivals.

A. Different components of channel delay spread

Reflections from the moving ocean surface as well as the sea bottom which functions as a diffuse reflector, lead to multipath arrivals from the transmitter to the receiver. This results in a non-stationary time-varying channel impulse response, popularly referred to as the delay spread,[1–6,8,9] which typically stretches over 100–200 delay taps (e.g., refer to results from experimental field data in Ref. 8).

Figure 1 shows a typical time-varying delay spread (∼30 msec long) of an UWA channel (estimated from field data of SPACE08 experiment, Sec. II of Ref. 13) at 15 m depth and 200 m range. Delay refers to delay taps constituting the channel impulse response at a given point in time on the x axis. The direct arrival path, the primary multipath region, and the secondary multipath region are marked in Fig. 1.

This is to note that the channel delay spread comprises three distinct arrival regions:

(1) The direct arrival representing the line-of-sight arrival of the acoustic waves from the transmitter to the receiving hydrophone. The direct arrival path manifests as the steady bright line at the bottom of Fig. 1, and is relatively constant over time, unless there is relative motion between the transmitter and receiver;
(2) Primary multipath reflections that are, typically, the combined effect of one or a few surface wave reflections.[1,8,11] These delay taps, henceforth referred to as the primary delay taps, are highly transient in nature. They occupy a significant fraction of the channel energy and

[a)]Electronic mail: naushada@iiitd.ac.in

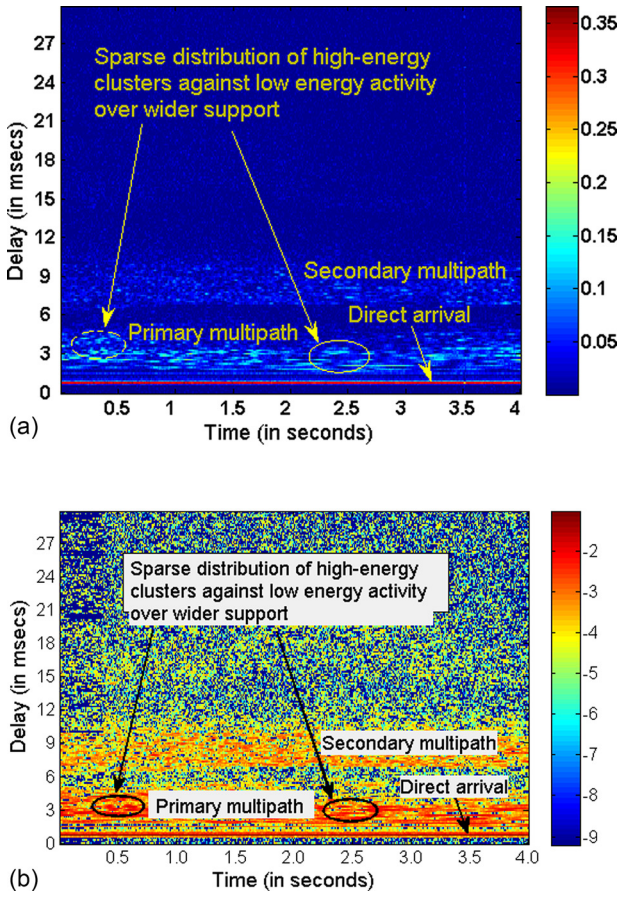

FIG. 1. (Color online) Shallow water acoustic channel [estimated from field data of SPACE08 experiment (Ref. 13)], plotted as a 2D image (Delay vs Time) showing significant time-variability in primary and secondary multipath regions. High-energy clusters of delay spread components in the primary multipath region are also pointed out (a) with linear colorbar (b) with log scale colorbar.

support, and occasionally exhibit high-energy peaks[12] and transient oceanographic events as highlighted in Fig. 1; and

(3) Secondary multipath reflections resulting from several reflections between the moving ocean surface and sea bottom. Due to attenuation at each reflection, these multipath arrivals do not have large energy within the delay spread, but collectively constitute a significant portion of the channel support. The secondary multipath arrivals are more relevant over medium range and shallow water depths as greater water depths and longer ranges attenuate their energy to ambient noise levels.

B. Uncertainty principles dictating underlying channel tap distribution

Non-stationary shifts in the channel delay spread due to oceanographic fluctuations limit the ability of adaptive signal processing techniques, with and without sparsity constraints, to track the shallow water channel in real time. In particular, uncertainty principle dictating localization of the non-stationary channel delay spread in time and frequency need to further consider the shifting sparseness of channel support.[11] The three-way uncertainty involving time, frequency, and sparsity across the transient delay taps render direct application of sparse sensing methods challenging in the shallow water domain. This is particularly true under moderate to rough sea conditions. Data-driven evidence of the shifting sparsity has been provided in Ref. 14.

C. Summary of related work and scope

The scope of this work is geared toward real-time channel estimation over medium ranges and shallow water depths, though signal processing techniques proposed here are equally applicable to greater water depths and longer ranges. The focus of this work is on the medium range because the joint effect of the primary and secondary multipath arrivals are most pronounced in this paradigm and hence, this is the more daunting scenario to solve. To provide field-driven evidence to the proposed methods, channel ground truths derived from experimental field data collected at 200 m range and 15 m depth are chosen as a representative scenario for this paradigm.

Localization of time-varying channel delay spread is challenging due to rapidly fluctuating multipath arrivals discussed in Sec. I A and uncertainty principles governing localization as discussed in Sec. I B. Current state-of-the-art in shallow water channel estimation addresses these challenges in four complementary thrusts:

(1) Non-uniform methods that attempt to discover and predict the shallow water channel using ray theory models;[1,15]
(2) Adaptive signal processing methods based on least-squared techniques;[1,6,16]
(3) Sparse recovery methods in optimization framework that exploit the sparse support of high-energy transients;[17–19] and
(4) Channel estimation using multiple input multiple output (MIMO) framework.[17,18,20]

Sparse recovery methods[21–23] are well-known to provide improvements over traditional adaptive least squares techniques,[24] when the signal to be recovered has sparse support. In such scenarios, regularization terms are added as constraints in the optimization framework to enable signal recovery.[25] Sparse recovery methods are closely tied but separate from Compressive Sampling/Compressed Sensing (CS)[26–29] techniques that solve the problem of signal recovery from an underdetermined system of linear equations under sparsity constraint. Recently, Orthogonal Matching Pursuit (OMP) and Compressive Sampling Matching Pursuit (CoSaMP) optimization methods have been employed to solve the channel estimation problem[17] wherein an underdetermined system of linear equations is solved under sparsity constraint. However, no compressive sensing *per se* has been carried out that targets the shallow water acoustic channel with its intricate interplay of multipath structure showing a non-uniform structure with varying degrees of sparsity between slow-varying components and rapid fluctuations. Furthermore, non-uniform channel impulse response (i.e., delay spread) due to multipath arrivals in UWAs communication provides background motivation to formulate the channel estimation problem in a compressive sampling framework.[17,18,20]

The confluence of adaptive signal processing, compressive sampling, and sparse recovery in the context of UWA communications is indeed encouraging and recently gained momentum in the shallow water acoustic communications literature.[1,6,14,16–18,20]

Motivated with the above discussion, the objective of this research is to contribute to this momentum with a two-dimensional (2D) frequency-domain formulation of the underwater channel that complements existing formulations and enables robust localization of dominant components of the fundamentally non-stationary shallow water acoustic channel.

As discussed above and elaborated in Ref. 11, the three-way uncertainty involving time, frequency, and sparsity provides localization challenges for direct application of sparse sensing methods with appropriate observation windows. As such, the precise localization of the shallow water channel in time, frequency, and sparsity is not possible without precise real-time knowledge of ocean ground truths that is impractical to determine in real-life experiments. Thus, accuracy of channel estimation is inherently tied to parameter localization within the three-way uncertainty constraints that drive field experiments. The key intuition is that, with suitable formulation, the dominant components of the shallow water channel may be localized robustly in real time. This work is aimed to address this fundamental localization and channel estimation challenge by bridging the above complementary approaches discussed in Sec. I C. Specifically, the inherent physical properties of a multipath within the shallow water channel are harnessed with adaptive sparse sensing approaches and partial sampling methods.

Key contributions of this work can be summarized as below:

(1) A 2D frequency domain representation is obtained via a carefully chosen transmitted signal design. This modeling transforms the problem of channel estimation to channel recovery in 2D Fourier domain. Interestingly, this framework is similar to *K*-space based image reconstruction used in Magnetic Resonance Imaging (MRI) where CS is used extensively as the default method for signal recovery. Similar to the MRI domain, the UWA channel (*vis-à-vis* signal in MRI) is sparse in the 2D Fourier domain. Figure 2 shows the 2D Fourier transform of the channel. While the existing sparse recovery methods in UWA channel estimation utilize sparseness of the channel in the time domain, the channel is sparser in the frequency domain. For example, refer to Fig. 3 which plots the sorted magnitude of coefficients of the channel (of Fig. 1) in the 2D time domain and the 2D frequency domain (Fig. 2). It is observed that the sorted magnitude of coefficients of channel in the 2D frequency domain drops off more rapidly as compared to that of coefficients of channel in the 2D time domain and hence, the channel is sparser in the 2D Fourier domain. Thus, the proposed frequency domain representation allows CS framework to be inherited naturally. Here, it is pertinent to add that this framework has been proposed for the first time in UWA and is a significantly novel contribution of this work.

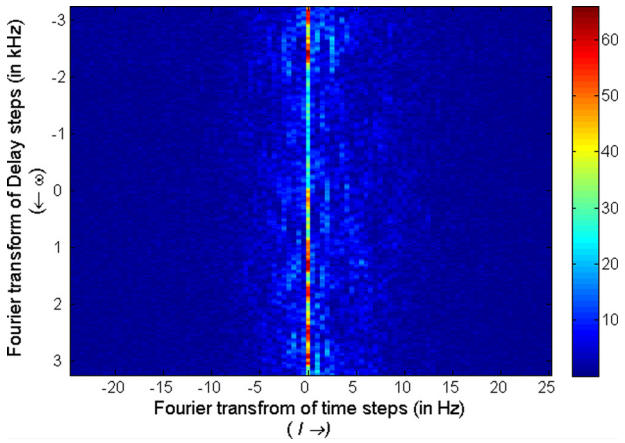

FIG. 2. (Color online) 2D Fourier Transform of channel in baseband [estimated from field data of SPACE08 experiment (Ref. 13)] shown in Fig. 1; Note: colorbar is linear.

(2) This paper introduces non-uniform compressing sampling for shallow water acoustic communications. Specifically, techniques presented in this work perform random compressive sampling at different sampling rates across different frequency bands in the 2D frequency domain. Later in this work, it has been shown that simply using CS framework with the basis pursuit denoising (BPDN) method does not yield good results because there is a need of detection of high-energy transients along with high-precision tracking of stationary but smaller delay taps. Thus, this paper proposes non-uniform compressive sensing with prior information and non-uniform modified-CS[30] with the prior information method for channel estimation wherein application domain knowledge is utilized with reference to frequency domain characteristics of the shallow water channel. Thus, this paper illustrates the use of CS methods but by appropriately rooting them in this application domain. It should be noted that some of the existing methods use the CS framework by setting up the problem as an underdetermined system of linear equations under sparsity constraint.[8,17,18] However, non-uniform compressing sensing has not been used *per se* in shallow water acoustic channel estimation. In particular, we present non-uniform compressive sampling that is cognizant of the intricate interplay of a multipath structure showing a non-uniform structure with varying degrees of sparsity between slow-varying components and rapid fluctuations. This work actually uses compressively sensed data for channel recovery.
(3) Extensive numerical validation of proposed techniques against existing techniques are provided based on channel estimates from field experiments as well as a public-domain channel simulator that has recently been tested against data from different field trials.

D. Organization, notation, and units

This paper is organized in five sections. Section II presents details of the experimental setup for ground truth on channel using channel estimates obtained from field experiments. Section III presents the proposed framework of

dictionary design and partial Fourier sampling for channel estimation along with the simulation results. This section considers transmission of dictionary signals over all frequency sub-channels for the purpose of channel estimation and employs non-uniform compressed sensing frameworks for channel estimation. This section presents results on SPACE08 channel data. Section IV presents results on another simulated channel obtained from a recently proposed channel simulator in order to further substantiate the proposed work. Section V summarizes results of this paper.

Notations. Lowercase bold letters denote vectors, uppercase bold letters denote matrices, and lowercase italics letters denote scalars.

Units. Unless stated otherwise, delay taps are expressed as numerical indices with appropriate time windows stated in msec and frequency units are given in Hz. Channel delay spread estimates are interpreted in voltage units. This is because the delay taps are most directly reflective of a "voltage" at the A/D converter and can be related to uPa at the receiver through hydrophone specifications.

II. EXPERIMENTAL SETUP FOR USING CHANNEL ESTIMATES FROM FIELD EXPERIMENTS

Numerical experiments presented in the work are based on channel simulations derived from two independent sources:

(i) Channel estimates employing the non-convex mixed norm solver (NCMNS) algorithm[8] on experimental field data collected using Binary Phase Shift Keying (BPSK)-signaling in the SPACE08 experiment conducted from October 18–27, 2008.[13] These channel estimates are used as ground truths for testing the efficacy of the proposed methods.

(ii) An independent channel simulator proposed recently[6,31] and unrelated to channel estimates in (i) above. This channel simulator is chosen because it models different multipath effects commonly encountered in shallow water acoustic communications, and has also successfully interpreted SPACE08 data as well as data from other field trials. Thus, the data from this simulator are used to demonstrate the generalization of results on shallow water channels from different sources.

A. SPACE08 experimental setup

The SPACE08 setup included one transmitter and four fixed receiving stations, each of which is equipped with several hydrophones, deployed at Martha's Vineyard Coastal Observatory (MVCO) and operated by Woods Hole Oceanographic Institution (WHOI). The experimental field data were collected in shallow waters at a depth of 15 m over a range of 200 m wherein the ocean floor of the area could be considered relatively flat and the temperature of the water column was constant. Multiple repetitions of a 4095 point BPSK modulated signal was transmitted at a symbol rate of 6.5 kbps at 13 kHz carrier frequency. For more details on the experimental setup, interested readers can refer to Ref. 13.

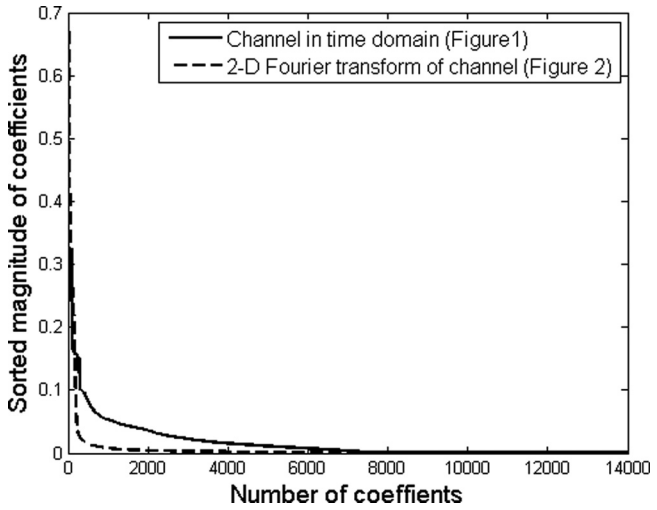

FIG. 3. Sorted magnitude coefficients of 2D time domain channel shown in Figs. 1 and 2D Fourier transform of channel shown in Fig. 2.

Figures 4 and 5 show channel estimates using Ref. 8, from the above mentioned experimental data, plotted as a function of time for 30 msec duration collected over moderate to rough sea conditions.

B. Justification for algorithm choice for obtaining channel estimates for SPACE08 data

Normalized prediction error is a robust statistical indicator of the true channel estimation error[32] and therefore, an accurate metric to measure efficacy of channel estimation techniques over experimental field data where the ground truth is unknown. NCMNS channel estimates are chosen in this work because NCMNS achieved minimum prediction error among several widely used competing sparse recovery techniques over the experimental field data collected in the SPACE08 experiment. An in-depth analysis of relative performance of different mixed norm algorithms over SPACE08 data as well as extensive computer simulations is provided in Ref. 8. In particular, the NCMNS technique provided best adaptability to sudden changes in the underlying distribution (Figs. 1 and 2 of Ref. 8), which is a practical challenge of shallow water acoustic channels due to

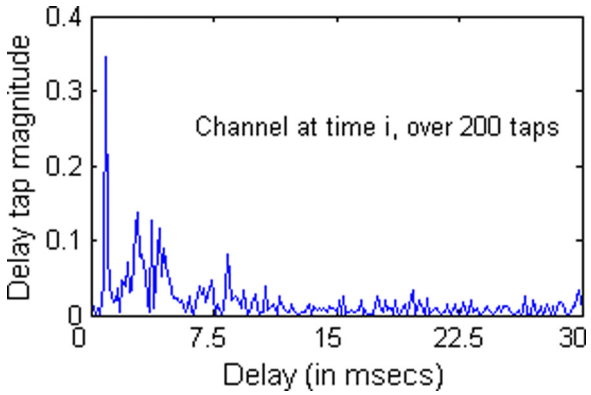

FIG. 4. (Color online) Representative channel estimates at time *i*, using Ref. 8 as kernel solver estimated from the field data of SPACE08 experiment (Ref. 13).

unpredictable multipath effects. This relative robustness of the NCMNS technique to unpredictable shifts is primarily due to agile navigation of the non-convex cost function, that offers faster convergence to multiple equivalent local minima that each represent the underlying channel scattering function (Secs. 4 and 5 of Ref. 8).

III. CHANNEL ESTIMATION EMPLOYING FREQUENCY-SELECTIVE NON-UNIFORM COMPRESISVE SAMPLING AT THE RECEIVER

In this section, a 2D frequency-domain characterization of the shallow water acoustic channel is introduced to facilitate channel estimation that is cognizant of slow and rapid temporal fluctuations across the channel components. Specifically, frequency-selective non-uniform compressive sampling is introduced, which exploits the 2D frequency characterization. The interesting outcome of the proposed framework is that it transforms the problem of channel estimation to non-uniform sparse recovery in 2D Fourier domain. A discussion of channel recovery using traditional compressive sampling (basic-CS) is also provided as background information on the related state-of-the-art.

A. Mathematical formulation of channel model in the 2D frequency domain

The following notations for channel parameters are introduced for the shallow water acoustic channel model, in addition to general notations discussed in Sec. I D:

- K: total number of delay taps;
- L: total number of Doppler frequencies;
- i: time index;
- k: delay tap index, $k = 0, 1, \ldots, K-1$;
- l: Doppler frequency (dual domain to time dimension) index, $l = 0, 1, \ldots, L-1$;
- ω: delay frequency (dual domain to delay dimension) index, *omega* is quantized to the same number of elements as delay taps, i.e., $\omega = 0, 1, \ldots, K-1$;
- $H[i, k]$, $k = 1, \ldots, K$: channel impulse response at time index i, measured at kth delay tap; Thus, $\mathbf{H}$ denotes 2D channel matrix in time-delay (i, k) domain;
- $\mathbf{U}$: 2D channel matrix in dual frequency or 2D frequency (l, ω) domain.

This section introduces a non-uniform compressive sampling and sparse recovery scheme that exploits the separation of non-sparse structure at low frequencies and the sparse structure at higher frequencies in the 2D frequency representation presented in the sequel [refer to Eq. (4)]. The key idea behind the mathematical formulation is that transmitted signals will be constructed as an orthogonal basis in (l, ω) domain, thus reducing the channel estimation problem to spectral sampling problem in the 2D Fourier domain.

Consider the complex exponential input signal $x[i, \omega] = e^{j(2\pi i\omega/K)}$, corresponding to delay frequencies $\omega = 0, 1, \ldots, K-1$ across parallel K number of sub-channels. These K sub-channels may be easily designed in baseband using appropriate frequency selective techniques. In addition, consider L Doppler frequencies $l = 0, 1, \ldots, L-1$ for sampling the channel in the Doppler domain. On transmission of the above designed input signal over the time-varying K-length channel impulse response $H[i, k]$, one obtains

$$\begin{aligned} y[i,\omega] &= \sum_{k=0}^{K-1} H[i,k]x[i-k,\omega] \\ &= \sum_{k=0}^{K-1} H[i,k]e^{j(2\pi(i-k)\omega/K)} \\ &= e^{j(2\pi i\omega/K)} \sum_{k=0}^{K-1} H[i,k]e^{-j(2\pi k\omega/K)}. \end{aligned} \tag{1}$$

On multiplying both sides of Eq. (1) with $e^{-j(2\pi i\omega/K)}$, one obtains

$$y[i,\omega]e^{-j(2\pi i\omega/K)} = \sum_{k=0}^{K-1} H[i,k]e^{-j(2\pi i\omega/K)}. \tag{2}$$

On computing the one-dimensional Fourier transform of the time variable i in Eq. (2), that corresponds to Doppler frequency, one obtains

$$\begin{aligned} U[l,\omega] &= \sum_{i=0}^{L-1} y[i,\omega]e^{-j(2\pi i\omega/K)}e^{-j(2\pi il/L)} \\ &= \sum_{i=0}^{L-1}\sum_{k=0}^{K-1} H[i,k]e^{-j(2\pi k\omega/K)}e^{-j(2\pi il/L)}, \end{aligned} \tag{3}$$

where Eq. (3) represents 2D Fourier transform of the channel impulse response $H[i, k]$, $\omega = 0, 1, 2, \ldots, K-1$ and $l = 0, 1, 2, \ldots, L-1$. Equation (3) can be re-written as

$$\mathbf{U} = \mathbf{F}_1\mathbf{H}\mathbf{F}_2 = \mathfrak{F}\mathbf{H}, \tag{4}$$

where $\mathbf{U}$ is the matrix form of $U[l, \omega]$ of size $L \times K$, $\mathbf{H}$ is the matrix form of channel impulse response $H[i, k]$ of size $L \times K$, $\mathbf{F}_1$ is the $L \times L$ Fourier transform matrix, $\mathbf{F}_2$ is the $K \times K$ Fourier transform matrix, and $\mathfrak{F}$ is the symbolic notation of the 2D Fourier transform operator.

The above formulation clearly shows that perfect channel recovery can be done in a noise free scenario via 2D inverse Fourier transform of the post-processed received signal $\mathbf{U}$. Thus, designing the transmitted signal and post-processing the received signal in the 2D (ω, l) domain has transformed the problem of channel estimation in time-domain to channel recovery from its salient spectral features: both along delay frequency dimension ω, signifying channel micro-structure, and the Doppler frequency dimension l, signifying fast or slowly varying trends. As discussed in the sequel, the support of these channel features, while exhibiting high spikes against the background, varies significantly between low and high Doppler frequencies, thus motivating the case for non-uniform compressive sampling in the 2D frequency domain.

Interestingly, this framework is similar to K-space based image reconstruction used in MRI.[33,34] CS is one of the most successful approaches in MRI image reconstruction where a

less number of MRI samples are sensed for reconstruction. This motivates us to explore CS based channel recovery in the proposed framework that is the focus of Sec. III B. This is to note that the above formulation is a completely new way of presenting channel estimation problem.

B. Justification for 2D Fourier representation

A snapshot of 2D Fourier transform or Fourier dual of delay spread and time is illustrated in Fig. 2. It is noteworthy that the 2D frequency representation shows clusters of slowly varying channel components across the low Doppler frequencies, while *variability along the impulse response structure of these slowly varying channel components are recorded along the* ω *axis*. The transient channel components are recorded along the higher Doppler frequencies. Key benefits behind this representation are threefold:

(i) Channel microstructure specific to slowly varying channel components gets highlighted along the ω (delay-frequency) axis; this allows high-precision recovery of these components, which are critical to effective underwater communication systems;
(ii) Slow-varying channel components, localized in lower Doppler frequencies, are easily disambiguated against rapidly fluctuating channel components localized in higher Doppler frequencies; and
(iii) This representation allows a non-uniform compressive sampling framework, where the slowly-varying components in the lower Doppler frequencies occupy a significantly broader support than the high-energy channel transients along the higher Doppler frequencies.

C. Partial Fourier sampling based channel estimation—Basic CS

In general, the received UWA signal will be corrupted with noise. This transforms the above problem to denoising based channel recovery in the 2D Fourier domain. Since additive white Gaussian noise (AWGN) will remain AWGN under any orthogonal transformation, it will remain AWGN under Fourier transform of the received signal in Eq. (3).

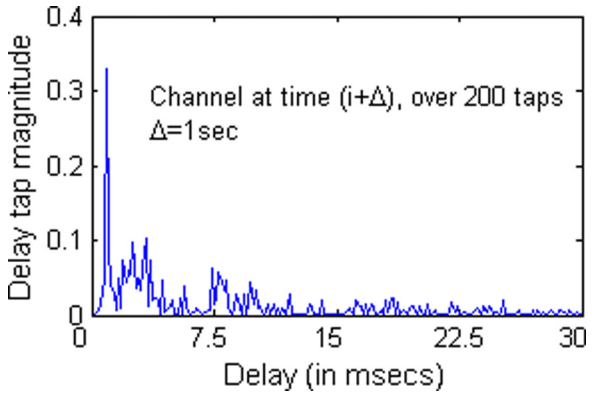

FIG. 5. (Color online) Representative channel estimates at time $(i+\delta)$, using Ref. 8 as kernel solver estimated from the field data of SPACE08 experiment (Ref. 13).

Thus, Eq. (4) can be re-written in the presence of noise as below

$$\mathbf{U}_n = \mathfrak{F}\mathbf{H} + \mathbf{N}, \tag{5}$$

where $\mathbf{U}_n$ is the noisy version of $\mathbf{U}$ and $\mathbf{N}$ is the complex white Gaussian noise matrix. Since channel $\mathbf{H}$ is known to be sparse in the underwater communication literature,[1,8] the problem can be formulated as the BPDN problem[35] and is, mathematically, given by

$$\min_{\mathbf{H}} ||\mathbf{H}||_1 \quad \text{subject to } ||\mathbf{U}_n - \mathfrak{F}\mathbf{H}||_2^2 \leq \sigma, \tag{6}$$

where $||\mathbf{V}||_1$ denotes the sum of the absolute values of $\mathbf{V}$, $||\mathbf{V}||_2^2$ denotes the sum of the squares of the values of $\mathbf{V}$, and σ is the standard deviation or the measure of the noise level.

Equivalently, the problem can also be modeled mathematically as

$$\min_{\mathbf{H}} ||\mathbf{U}_n - \mathfrak{F}\mathbf{H}||_2^2 \quad \text{subject to } ||\mathbf{H}||_1 \leq \tau. \tag{7}$$

The above formulation is termed as the Least Absolute Shrinkage and Selection Operator (LASSO)[25] and τ is the measure of the sparsity of the channel $\mathbf{H}$. Incorporating the theory of CS, channel $\mathbf{H}$ can be estimated using partial Fourier sampling of $\mathbf{H}$ as explained below.

Consider the compressively sensed version of $\mathbf{U}$ as below

$$\mathbf{U}_{\text{sub}} = \Re\mathfrak{F}\mathbf{H} + \mathbf{N}, \tag{8}$$

where $\mathbf{U}_{\text{sub}}$ is the sub-sampled and noisy measurement of $\mathbf{U}$ and $\Re$ is the random binary sub-sampling operator or a matrix consisting of 1's and 0's that allows random selection of positions in the 2D Fourier domain leading to different sampling ratios. $S\%$ sampling ratio implies $\lfloor LK \times S/100 \rfloor$ number of samples is being captured randomly. The channel recovery in denoising-based basic CS framework can be formulated as

$$\min_{\mathbf{H}} ||\mathbf{U}_{\text{sub}} - \Re\mathfrak{F}\mathbf{H}||_2^2 \quad \text{subject to } ||\mathbf{H}||_1 \leq \tau. \tag{9}$$

From Figs. 1, 4, and 5, it can be noted that channel exhibits fewer areas of high activity that dominate over lower and diffused spread of smaller taps. Interestingly, it is noticed from Figs. 2 and 5 that the 2D Fourier transform of channel, i.e., $\mathfrak{F}\mathbf{H}$ is sparser than the channel itself. Thus, it is proposed to estimate channel $\mathbf{H}$ in the CS based denoising framework considering the sparsity of $\mathbf{U}$ as below

$$\min_{\mathbf{U}} ||\mathbf{U}_{\text{sub}} - \Re\mathbf{U}||_2^2 \quad \text{subject to } ||\mathbf{U}||_1 \leq \tau, \tag{10}$$

where $\mathbf{U} = \mathfrak{F}\mathbf{H}$ and τ is the measure of the sparsity of $\mathbf{U}$.

In the following experiments, the value of τ is set to $0.5\sqrt{LK}$, where L is the granularity of Doppler frequencies and K is the number of delay frequencies. This value of τ is found to provide a good estimate of channel in all the experiments presented in this paper and is found empirically.

Figure 6 shows the variation of the normalized mean squared error (NMSE) of reconstructed channel with c, where $\tau = c\sqrt{LK}$ for three window length, 7.68, 9.22, and 10.75 msec. The experiment is carried out at the 70% sampling ratio at noisy channel signal-to-noise ratio (SNR) of 5 dB. This figure illustrates that NMSE is reasonably low with $c = 0.5$ or when $\tau = 0.5\sqrt{LK}$ for all three window lengths. The same scenario is observed with all other results in the sequel and hence, this value of τ is chosen.

The problem has been solved with the MATLAB toolbox SPGL1.[36,37]

In order to test the performance of the proposed channel estimation method with basic CS, Monte Carlo simulations are carried out over 200 iterations for each noise level. The performance is evaluated via NMSE measured in decibels (dB). Results are displayed over additive white complex Gaussian noise of varying variance. In addition, different window lengths are considered for channel estimation. The SNR of noisy channel is computed as below

$$\text{SNR of Noisy Channel} = 10\log_{10}\left(\frac{\frac{1}{LK}\sum_{i=0}^{L-1}\sum_{k=0}^{K-1}|H(i,k)|^2}{\sigma_n^2}\right), \quad (11)$$

where σ_n^2 represents the noise variance.

The NMSE of estimated channel $\hat{H}[i,k]$ measured in dB is computed as below

$$\text{NMSE} = 10\log_{10}\left(\frac{\sum_{i=0}^{L-1}\sum_{k=0}^{K-1}|H(i,k)-\hat{H}(i,k)|}{\sum_{i=0}^{L-1}\sum_{k=0}^{K-1}|H(i,k)|^2}\right). \quad (12)$$

Figures 7 and 8 represent NMSE results on channel recovery using the basic CS approach given in Eq. (10). Corresponding to CS, impact of varying sampling percentage in the 2D Fourier domain on channel recovery is studied. As the SNR decreases from 10 to 5 dB, an increase in NMSE is observed with a most pronounced increase (~3 dB) at a 100% sampling ratio. Further, it is observed that the sampling ratio increase leads to progressively superior performance, with the lowest NMSE attained at 100% (i.e., no compressive sampling that is actually *sparsity-constraint least squares*). Thus, it is concluded that traditional compressive sampling as used in Eq. (10) does not lead to good channel recovery.

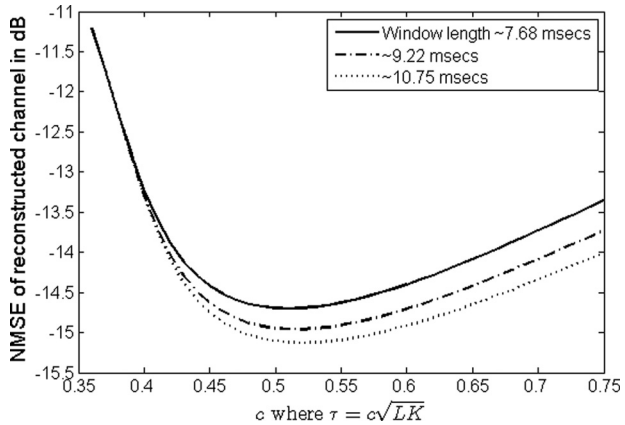

FIG. 6. Reconstruction accuracy of channel in terms of NMSE versus the value of c where $\tau = c\sqrt{LK}$.

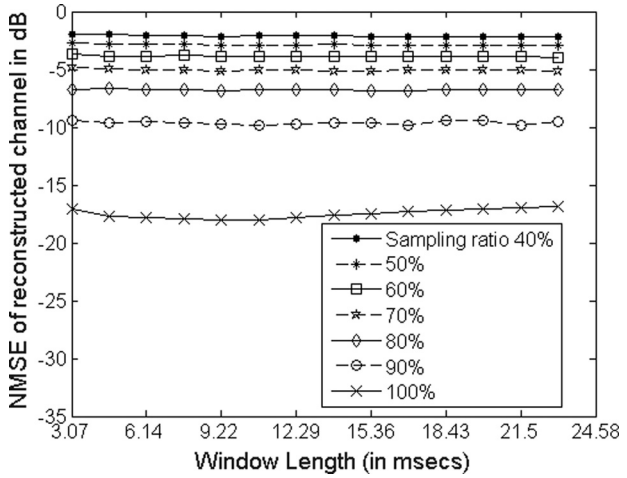

FIG. 7. NMSE results on channel estimation using the traditional CS at noisy channel SNR of 10 dB; implements Eq. (10).

D. Proposed channel estimation using compressive sensing with prior information

In Sec. III C, it is observed that the traditional CS without modifications is unable to recover the channel. Thus, it is proposed to introduce channel-cognizant constraints to improve estimator's performance. First, consider the following observations from Figs. 1–5:

(1) Direct arrival and primary multipath regions dominate the channel support (Figs. 1 and 2).
(2) The zero Doppler frequency column $\mathbf{U}[0,\omega]_{\omega=0}^{K-1}$, in Fig. 2 is the most dominant component of the channel. Physically, it represents the time-invariant slowly

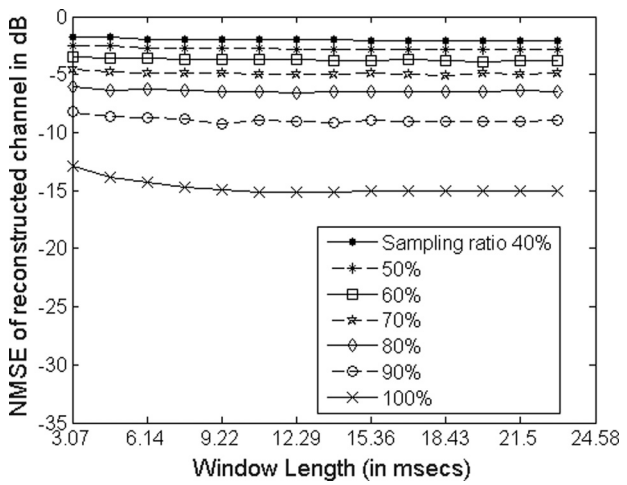

FIG. 8. NMSE results on channel estimation using the traditional CS at noisy channel SNR of 5 dB; implements Eq. (10).

changing component due to direct arrival and persistent multipath arrivals.

(3) Rest of the support $\mathbf{U}[l \neq 0, \omega]_{l=1,\omega=0}^{L-1,K-1}$ is dominated by slower Doppler frequency components, particularly, $\mathbf{U}[\pm 1, \omega]_{\omega=0}^{K-1}$.

(4) Rapidly fluctuating multipath arrivals (observed in higher numbered delay taps in Fig. 4 and Fig. 5) occupy high-frequency columns of $\mathbf{U}[l \neq 0, \omega]_{l=2,\omega=0}^{L-1,K-1}$ as high-energy components, i.e., for $l \geq 2$.

The above observations imply co-existence of dominant slowly varying component and high-energy transients owing to ephemeral oceanic events.[12] Another possible reason for high-energy transients can be constructive interference from multipaths due to intersecting surface waves. Current sparse sensing literature[21–23] as well as the proposed framework in Sec. III C ignores these physical constraints posed on $\mathbf{U}[l, \omega]_{l=0,\omega=0}^{L-1,K-1}$ due to multipath propagation in the shallow water acoustic paradigm.

This establishes motivation for employing acoustic physics-cognizant channel knowledge to densely sample in the zero- and low-Doppler frequency regions that correspond to dominant oceanographic activity. This proposed framework is hereby called non-uniform compressive sensing with prior knowledge.

In order to formulate it mathematically, assume that T denotes the support of $\mathbf{U}$ that contains dominant slowly varying components of the channel. All samples on the support T are considered and partial sensing is carried out on $|T^c| = n - |T|$, where $|.|$ denotes the cardinality of a set and n denotes the dimension of $\mathbf{U}$. Subsequently, channel $\mathbf{H}$ is estimated in CS with prior information based denoising framework as below

$$\min_{\mathbf{U}} ||\mathbf{U}_{\text{sub}} - \Re_{T^c}\mathbf{U}||_2^2 \quad \text{subject to} \quad ||\mathbf{U}||_1 \leq \tau, \tag{13}$$

where $\mathbf{U} = \mathfrak{F}\mathbf{H}$ and $\Re_{T^c}$ denotes restricted sampling operator that does partial sensing on T^c.

1. Frequency-selective noise suppression using Eq. (13)

Sparse recovery using Eq. (13) differs from the traditional CS formulation Eq. (10) in two significant ways:

(a) Sparse recovery is imposed on the entire space, i.e., the solution is heavily biased toward picking the highest components of the channel across the whole support.

(b) Partial sampling is limited to outside the main support.

In order to test bullet point (b) above, results are presented on the SPACE08 channel with no partial sampling or full sampling of zero Doppler in Figs. 9 and 10 and, full sampling of zero Doppler and first low-Doppler frequency columns in Figs. 11 and 12. The combination of these two criteria biases the channel recovery solution in Eq. (13) toward selecting the frequency channel components belonging to the main support of the channel, e.g., in this case the zero and low Doppler frequency components. This is partly due to the dominance of these components over the rest of the support as well as noise averaging over the lower frequency components, relative to higher frequency transients. Therefore, channel components in higher frequency region represented by outer columns experience a lower SNR compared to channel components in inner columns due to different rates of noise averaging. This leads to frequency-selective noise suppression using sparse recovery techniques along the l axis. It is noteworthy that the exact choice of what constitutes low Doppler depends on the state of the ocean, e.g., for really rough ocean with high wind activity, significant surface wave phenomena can push the choice of low Doppler boundaries [5–10 Hz] to higher ranges.

For the experimental SPACE08 field data used in this section, limiting Doppler activity observations to only ± 1 column next to zero Doppler was sufficient for capturing most multipath activity leaving outer columns for high-transient observations. The low-Doppler region of the channel is notated as $U[|l| \leq \theta, \omega]_{l=0,\omega=0}^{\theta,K-1}$, where θ is the chosen upper bound of the low Doppler frequency range. Choosing $\Re_{T^c}$ with a smaller sampling ratio will select all the dominant low-frequency activity around $U[|l| \leq \theta, \omega]_{l=0,\omega=0}^{\theta,K-1}$ and select only some of the high-energy components from the rest of the support.

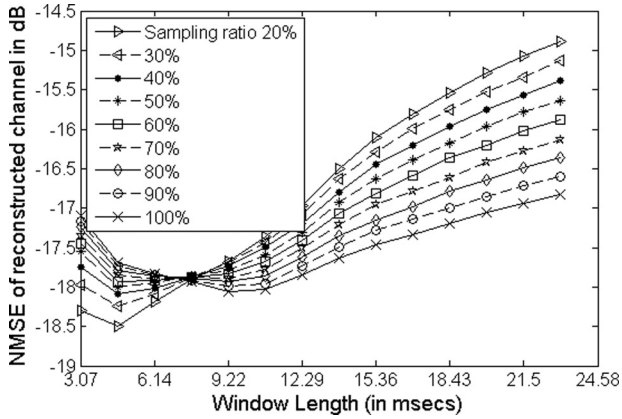

FIG. 9. NMSE results on channel estimation using CS with prior information, i.e., with full sampling of zero Doppler frequency; with noisy channel SNR = 10 dB; implements Eq. (13).

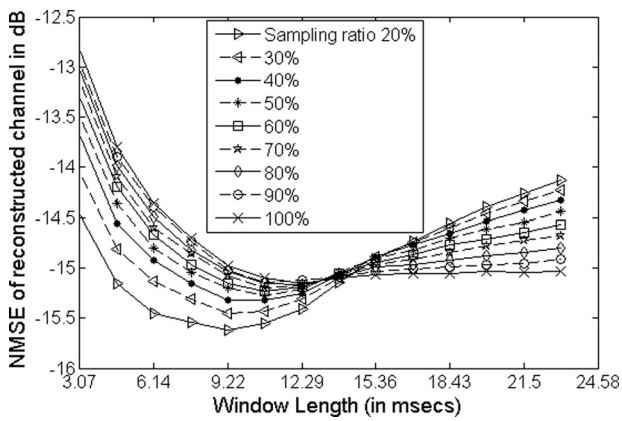

FIG. 10. NMSE results on channel estimation using CS with prior information, i.e., with full sampling of zero Doppler frequency; with noisy channel SNR = 5 dB; implements Eq. (13).

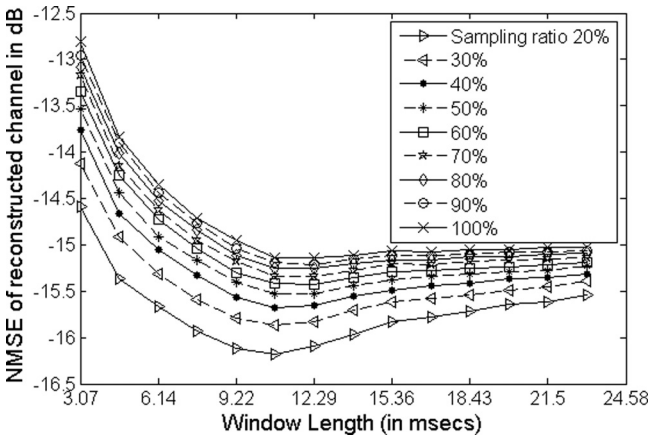

FIG. 11. NMSE results on channel estimation using CS with prior information, i.e., with full sampling of zero- and first low-Doppler frequency; with noisy channel SNR = 5 dB; implements Eq. (13).

NMSE results on channel estimation are presented considering full sampling in:

(a) zero Doppler frequency region of **U** at 10 dB (Fig. 9) and 5 dB (Fig. 10) of noisy channel SNR,
(b) zero Doppler and first (± 1) column adjacent to zero Doppler at 5 dB noisy channel SNR (Fig. 11), and
(c) zero Doppler and first two columns (± 2) adjacent to zero Doppler components at 5 dB noisy channel SNR (Fig. 12).

In Figs. 9–12, a clear minimum error is observed for each sampling ratio, even though the minimum may be achieved over different observation windows. This is due to the inherent uncertainty principle governing time, frequency, and sparsity localization, discussed in Ref. 11 The minimum is achieved when the observation window is long enough to capture $U[0,\omega]_{\omega=0}^{K-1}$, i.e., the zero-Doppler column precisely, for the given sampling ratio. Beyond this point, increasing the observation window length will not add to the precision of detecting $U[0,\omega]_{\omega=0}^{K-1}$ but may reduce the precision of estimating higher Doppler columns, as high-energy transients may get averaged over longer window choices.

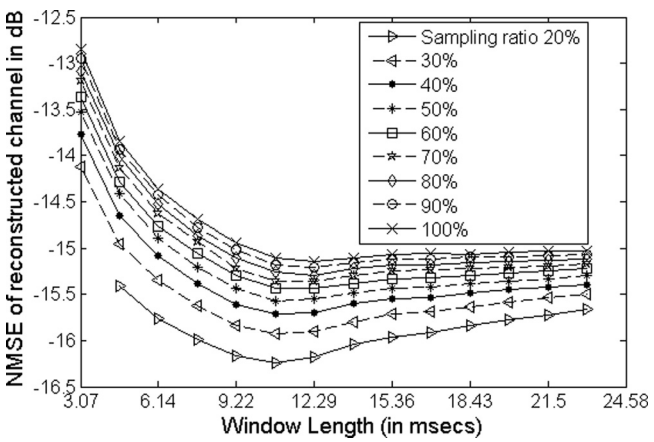

FIG. 12. NMSE results on channel estimation using CS with prior information, i.e., with full sampling of zero- and first two low-Doppler frequencies; noisy channel SNR = 5 dB; implements Eq. (13).

Further discussion of results regarding relative performance between different sampling ratios are given below.

2. Understanding NMSE behavior with different sampling ratios

In order to further understand NMSE results on channel estimation using CS with prior information, the performance of Figs. 9 and 10 are compared with those of Figs. 7 and 8 for noisy channel SNR = 10 and 5 dB, respectively. Significantly improved performance is observed over the traditional basic CS. This is to be expected as Eq. (10) is agnostic of channel support and blindly attempts recovery of the channel based on sparsity defined randomly over the whole space. On the other hand, Eq. (13) assumes basic physical knowledge of the channel support and therefore, samples it more efficiently.

Further, it is observed that NMSE converges across all sampling ratios to a cross-over point in Figs. 9 and 10 as the observation window increases followed by a reversal in performance across the sampling ratios in terms of NMSE performance. This is attributed to the NMSE Eq. (14) being dominated by the error in estimating the zero-Doppler column $U[0,\omega]_{\omega=0}^{K-1}$, as demonstrated by Tables I and II,

$$\mathrm{NMSE(in\,dB)} = 10\log_{10}\left(\frac{\sum_{\omega=0}^{K-1}|U(i,\omega)-\hat{U}(i,\omega)|^2}{\sum_{\omega=0}^{K-1}|U(i,\omega)|^2}\right), \tag{14}$$

where i corresponds to

(a) column (a) in Tables I and II—zero Doppler or the center column of Fig. 2,
(b) column (b) in Tables I and II—squared sum of errors in the I column to the left and right of the center column (zero Doppler) of Fig. 2, and
(c) column (c) in Tables I and II—squared sum of errors in the II column to the left and right of the center column (zero Doppler) of Fig. 2.

Channel recovery with the smallest sampling ratio (40%) recovers the zero-Doppler column $U[0,\omega]_{\omega=0}^{K-1}$ fastest, due to heavy noise suppression along the higher Doppler columns (Sec. III D 1), whereas higher sampling ratios need to

TABLE I. NMSE in dB in channel estimation in certain columns (SNR = 10 dB).

Window length	Sampling ratio (in %)	NMSE in zero Doppler column (a)	NMSE in first Doppler column (b)	NMSE in second Doppler column (c)
30	40	−24.3629	−1.237	−0.9177
30	100	−22.2622	−2.0794	−1.3027
50	40	−25.4511	−1.4963	−0.8712
50	100	−23.4827	−2.9483	−1.2379
70	40	−26.21	−1.8396	−0.9369
70	100	−24.2814	−4.0119	−1.3836

TABLE II. NMSE in dB in channel estimation in certain Doppler columns (SNR = 5 dB).

Window length	Sampling ratio (in %)	NMSE in zero Doppler column (a)	NMSE in first Doppler column (b)	NMSE in second Doppler column (c)
70	40	−21.2888	−1.142	−0.5903
70	100	−19.6378	−2.0201	−0.8047
90	40	−21.8233	−1.3136	−0.6645
90	100	−20.274	−2.5956	−0.996
110	40	−22.2825	−1.5632	−0.751
110	100	−20.7156	−3.2496	−1.1618

observe the channel longer to resolve noise suppression. This is further evidenced by the shift in the cross-over point from approximately 7 msec in Fig. 9 to approximately 13 msec in Fig. 10 as the SNR is decreased from 10 to 5 dB.

Figures 11 and 12 correspond to full sampling of zero and first Doppler columns, i.e., $U[|l| \leq 1, \omega]_{l=0,\omega=0}^{1,K-1}$ (Fig. 11) and zero Doppler and first two Doppler columns, i.e., $U[|l| \leq 2, \omega]_{l=0,\omega=0}^{2,K-1}$ (Fig. 12). Figures 11 and 12 do not display a significant difference because activity from second Doppler column, i.e., $U[|l| = 2, \omega]_{\omega=0}^{K-1}$ is not that significant relative to energy in $U[0, \omega]_{\omega=0}^{K-1}$. Both figures exhibit a progressively lower NMSE for smaller sampling ratios, without any cross-over point like in Figs. 9 and 10. This is to be expected, as all estimators in both figures sample the lower Doppler columns, i.e., $U[|l| \leq \theta, \omega]_{l=0,\omega=0}^{\theta,K-1}$ with a 100% sampling ratio ($\theta = 1$ for Fig. 11 and $\theta = 2$ for Fig. 12). In Figs. 11 and 12, sampling ratios differ only across higher Doppler frequency columns that capture high-energy transients and other ephemeral events. Thus, both these figures demonstrate a similar performance in channel estimation. The difference in performance across different sampling ratios as well as between corresponding curves in Figs. 11 and 12 depend only on the ability of the algorithm to pick up transient multipath energy at higher frequencies. The lower sampling ratios are heavily biased toward capturing only the high-energy transients in this domain due to their superior noise suppression and hence, achieve a lower NMSE than higher sampling ratios. Furthermore, higher energy transients average out with increasing window length, and hence, the performances of all estimators deteriorate after achieving minimal NMSE point at approximately 10.8 msec.

The above analysis shows that one needs to choose the appropriate window length and the appropriate sampling ratio in order to perform channel estimation. From Figs. 11 and 12, it is observed that when the observation window is long enough to capture slowly varying components, the performance of the method stabilizes, i.e., increasing the window length beyond, say, 9.22 msec does not change performance much. Figure 13 shows NMSE vs noisy channel SNR for window length from 6.14 to 15.36 msec using CS with prior information, i.e., with full sampling of zero- and first two low-Doppler frequency and overall sampling ratio of 70%. It is observed that curves of different window lengths run almost together between nearly 5–10 dB of noisy

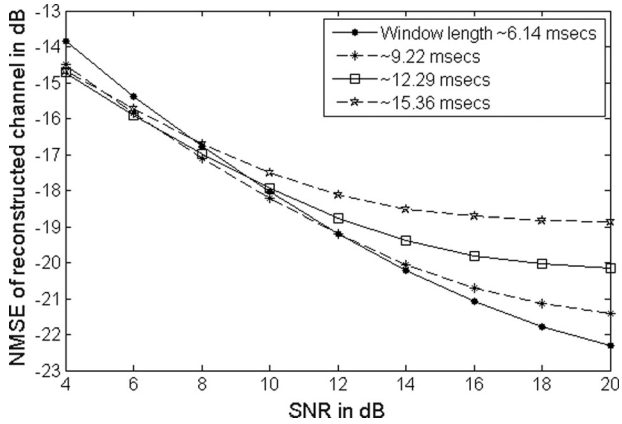

FIG. 13. NMSE vs noisy channel SNR using CS with prior information, i.e., with full sampling of zero- and first two low-Doppler frequency and with 70% sampling ratio; at different window lengths.

channel SNR. Thus, any window length between 9.22 to 15.36 msec is appropriate to provide good performance at these SNRs.

Figure 14 shows the variation of NMSE versus sampling ratio at a noisy channel SNR of 5 dB (corresponding to Fig. 12) to carefully look at the impact of the sampling ratio on NMSE at different window lengths. It is observed that at 5 dB channel SNR, window lengths from 10.75 to 23.04 msec provide almost a consistent performance from 60% sampling ratio onwards (with an NMSE change within ±0.5 dB). Better performance is observed at lower sampling ratios with an improvement of 0.5 to 0.8 dB compared to a 100% sampling ratio because the channel is sparse in the 2D frequency domain where the proposed CS based method is applied. Also, since the channel SNR is low (5 dB), the channel is noisy and hence, a lower sampling ratio will help in picking less but higher energy transients that are more likely to be higher SNR points in the frequency domain.

3. Adaptive approach to selecting observation window length and sampling ratio

An adaptive approach similar to Ref. 14 is presented for appropriate selection of the observation window length and

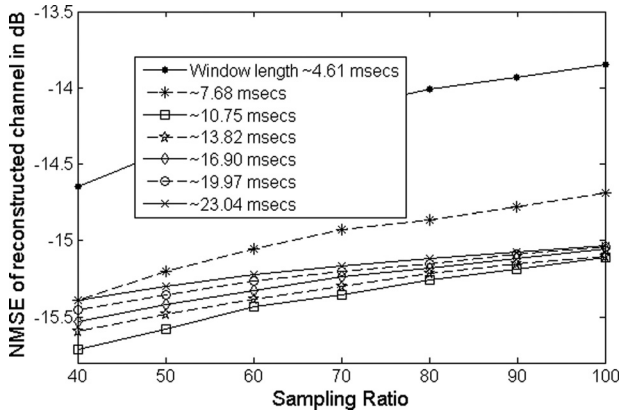

FIG. 14. Perturbation analysis for the case when full sampling is done of zero- and first two low-Doppler frequency with noisy channel SNR = 5 dB (i.e., corresponding to Fig. 12).

sampling ratio that minimizes the normalized prediction error. The approach is described in steps as follows:

(a) Step 1: Initialize window length and sampling ratio at some point, called the current operating point.
(b) Step 2: Choose window length on either side of the current operating point. If the prediction error decreases, go until the optimum point is reached.
(c) Step 3: Choose the sampling ratio on either side of the current setting and move in the direction of decrease of NMSE and choose the one with minimum NMSE.

E. Proposed channel estimation using *modified* CS with prior information

Section III D utilized non-uniform CS with prior information. In addition to the observations made in Sec. III D, it can be noted from Fig. 2 that Fourier transform of the channel $\mathbf{U}$ is sparser on the support T^c rather than the entire support (refer to Fig. 15). So, imposing the sparsity of $\mathbf{U}$ on T^c, unlike Eq. (13) that imposes sparsity on the entire support of $\mathbf{U}$, can increase the performance of channel estimation. This can be easily formulated in the context of modified CS.[30] Here, non-uniform modified CS with full sampling of zero Doppler frequency component of the channel transform $\mathbf{U}$ is utilized. In addition, the support of $\mathbf{U}$ is split into two non-overlapping subspaces S_1 and S_2:

(a) Subspace S_1 corresponds to support T^c where sparsity is imposed and partial sampling is carried out. This subspace is noisy and sparse, and corresponds to multiple reflections between the ocean surface and rough sea bottom, transient signal spikes from unpredictable wave focusing events, and low energy fluctuations due to attenuated multipath arrivals.
(b) Subspace S_2, the less noisy subspace complementary to (i) above, i.e., support T, where neither partial sampling is done nor sparsity is imposed. This subspace corresponds to relatively stable and higher-energy components that occupy the low-Doppler regions.

The proposed modified CS with prior information framework is now formulated as below

$$\min_{\mathbf{U}} ||\mathbf{U}_{\text{sub}} - \Re_{T^c}\mathbf{U}||_2^2 \quad \text{subject to} \quad ||\mathbf{U}_{T^c}||_1 \leq \tau, \tag{15}$$

where $\mathbf{U} = \mathfrak{F}\mathbf{H}$ and $\Re_{T^c}$ is the restricted sampling operator that does partial sensing on T^c. Channel estimation results are presented using the modified CS approach considering support T to be zero Doppler frequency region of $\mathbf{U}$ at 10 dB (Fig. 16) and 5 dB (Fig. 17) of a noisy channel SNR.

F. Discussion of results

Figures 16 and 17 present NMSE results with *modified CS with prior information* as given in Eq. (15) and reveal that a lower NMSE is achieved with a 100% sampling ratio compared to a 40% sampling ratio. This is to be expected as the contribution of the high-energy regions in the low-Doppler frequency space S_2 is explicitly accounted for in the sparsity and partial sampling considerations in Eq. (15), unlike Eq. (13). Thus, due to explicit prior setting in Eq. (15) lower sampling ratios do not offer any bias toward estimating the high-energy low-Doppler components. Furthermore, the partial sampling operator $\Re_{T^c}$ only captures sparsity in S_1 while suppressing background noise. Also, these results are in consonance with compressive sensing theory, whereby, the 100% sampling ratio provides the lowest NMSE and NMSE increases with decreasing sampling ratio.[38,39]

G. Comparative results

In this section, comparative results on channel estimation are presented with direct denoising based framework, i.e., least squares with sparsity regularization,[40] traditional basic CS (Sec. III C), CS with prior information (Sec. III D),[41] and modified CS with prior information (Sec. III E). In traditional basic CS, CS with prior information, and modified CS with prior information, partial sampling is employed at the receiver end. A key novelty of this work is the 2D Fourier domain representation of the UWA channel, which

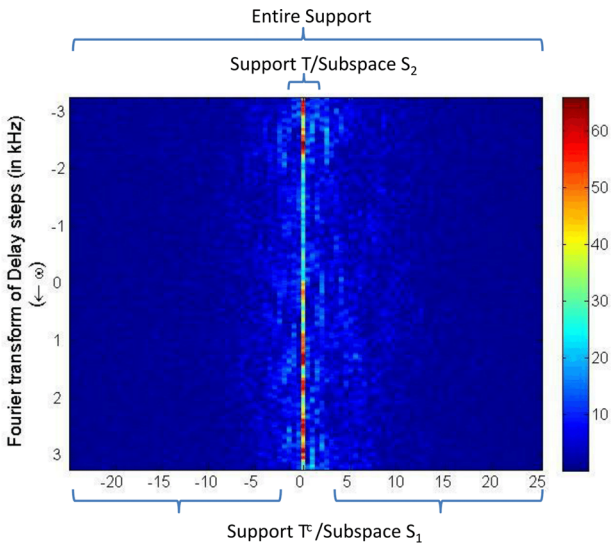

FIG. 15. (Color online) 2D Fourier representation of channel with labeling of subspaces and support.

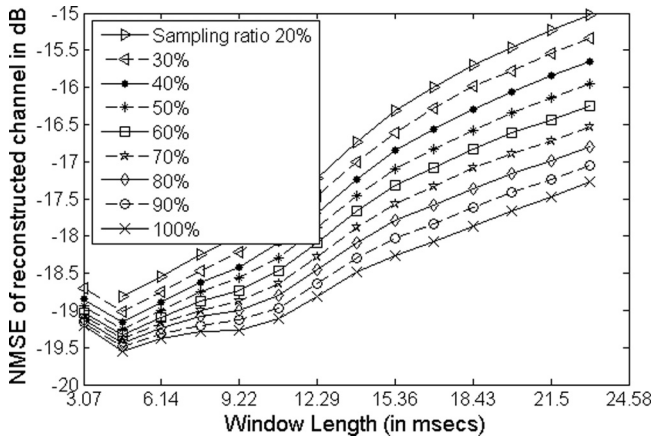

FIG. 16. NMSE results on channel estimation at 10 dB SNR with modified CS, support T is zero Doppler frequency; implements Eq. (15).

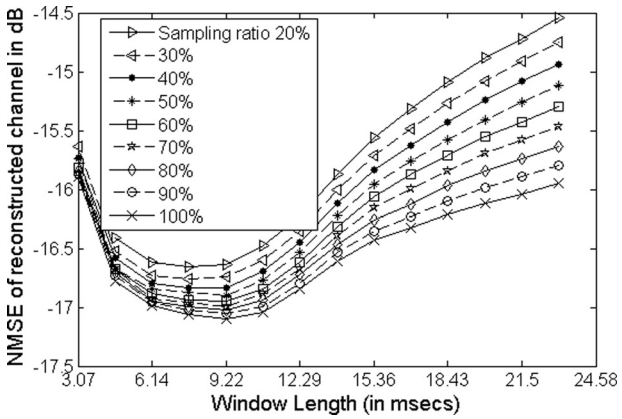

FIG. 17. NMSE results on channel estimation at 5 dB SNR with modified CS, support T is zero Doppler frequency; implements Eq. (15).

enables localization of slowly-varying channel components against transient and potentially high-energy taps due to ephemeral oceanic events. For the current 2D Fourier domain setting, traditional basic CS within this framework (Figs. 7 and 8) and least squares with sparsity regularization (direct denoising framework) are considered as the base performance standards to ensure a fair comparison against the state-of-the-art.

Figures 18 and 19 present NMSE results of an estimated channel with different window lengths and varying sampling ratios for noisy channel SNRs of 10 and 5 dB, respectively. It is observed that the *modified CS with prior information*, i.e., with full sampling of zero Doppler, Eq. (15) provides the best performance with a marginal performance gap between 40% and 100% sampling ratios. This is to be expected given the results and related discussions in Secs. III D and III E.

IV. RESULTS ON SIMULATED CHANNEL

In order to demonstrate the efficacy of the proposed method, this section presents results on a public-domain

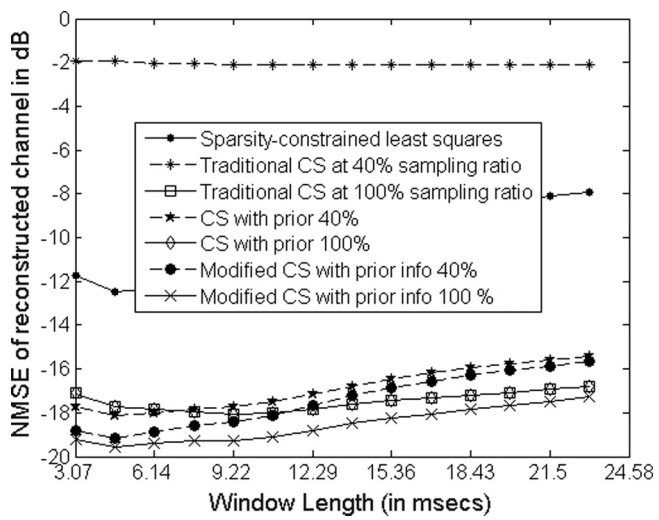

FIG. 18. Comparative performance of channel estimation with different sparse sensing techniques at 10 dB SNR; results on modified CS with prior relate to full sampling of zero Doppler.

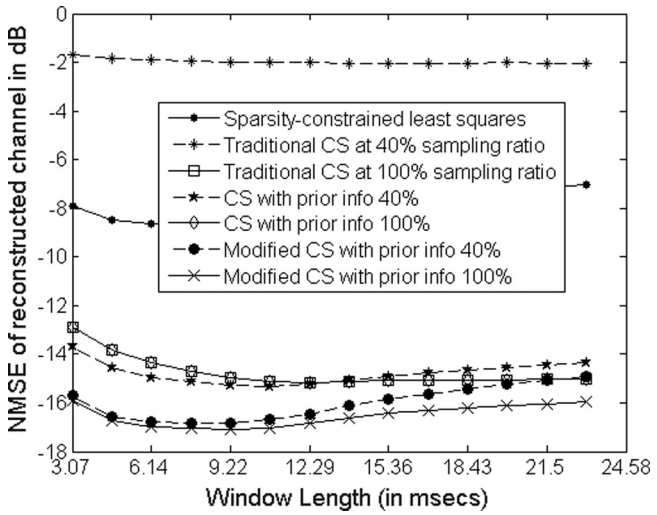

FIG. 19. Comparative performance of channel estimation at 5 dB SNR; results on modified CS with prior relate to full sampling of zero Doppler.

simulated channel that emulates multipath channel effects. This channel simulator has been proposed recently[6,31] and is unrelated to channel estimates used in Sec. III above. This channel simulator models different multipath effects commonly encountered in shallow water acoustic communications, and has also successfully interpreted specular reflections and multipath arrivals in the shallow water channel across several field trials[6,31] including SPACE08 and other experimental channel data. Channel parameters used in this simulation work are presented in the Appendix. A 2D delay-time snapshot of channel for 0.5 s duration is shown in Fig. 20 with corresponding 2D Fourier domain representation shown in Fig. 21.

Figures 20 and 21 clearly show that this channel is very distinct from the NCMNS channel estimates used for numerical simulations setup in Sec. III (refer to Figs. 1 and 5). Figure 22 shows a sorted magnitude of 2D time domain and 2D frequency domain channel coefficients. Compared to the 2D time-domain, this channel is also sparser in the 2D frequency domain, although the relative sparsity is less compared to the previous SPACE08 experimental data.

Channel estimation results are presented on this channel with modified CS with prior information. As evident from

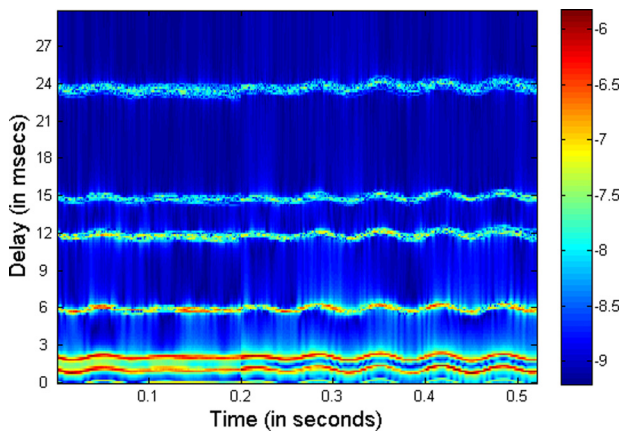

FIG. 20. (Color online) Simulated channel in delay-time (2D time domain) using Channel Simulator (Ref. 31); colorbar is in log scale.

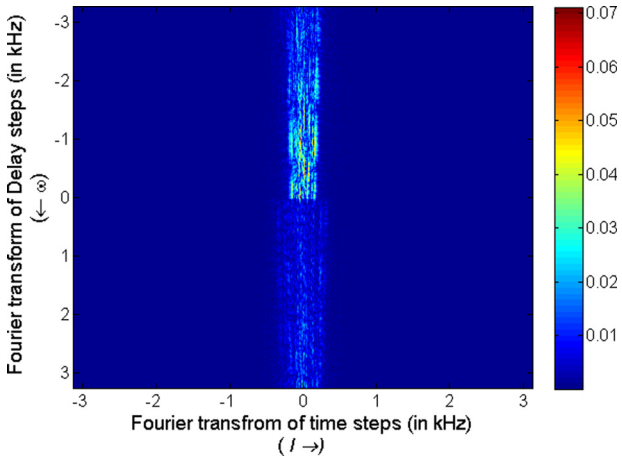

FIG. 21. (Color online) Simulated channel of Fig. 20 in 2D Fourier domain; colorbar is in linear scale.

Fig. 21, this channel is dense at zero Doppler and few low Doppler frequencies. Hence, the support T is considered to be zero Doppler and first five Doppler frequencies. NMSE estimation results are presented for noisy channel SNR of 10 and 5 dB in Figs. 23 and 24, and correspond to results presented in Figs. 16 and 17, which were based on simulations using NCMNS estimates on SPACE08 field data (200 m range, 15 m depth, moderate sea conditions). Similar to the results on a previous channel (Figs. 16 and 17), good results are obtained with the proposed non-uniform modified CS with prior information.

It is observed that for this independent numerical experiment, the NMSE variation shows two consistent similarities between Figs. 16 and 23: (i) NMSE performance of all sampling ratios converge up to a critical averaging window, which represents the minimum observation length to capture the dominant "steady-state," i.e., slowly varying channel components corresponding to low Doppler frequencies. (ii) While the lowest NMSE is obtained for the highest sampling rate, the difference in NMSE performance between different sampling ratios is within 1 dB for observation windows close to this critical window length.

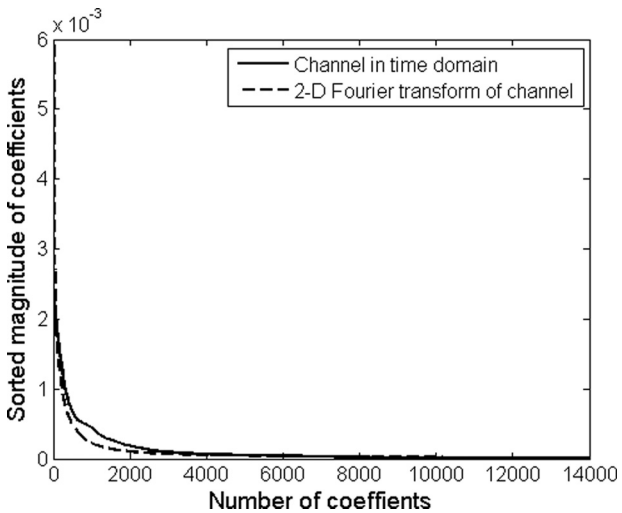

FIG. 22. Sorted magnitude coefficients of 2D time domain channel shown in Figs. 20 and 2D Fourier transform of channel shown in Fig. 21.

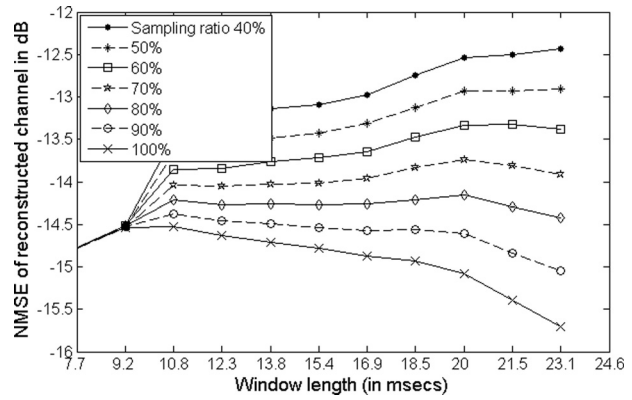

FIG. 23. NMSE results on channel estimation at 10 dB SNR with modified CS, support T is zero and first five non-zero Doppler frequencies; implements Eq. (15).

Lowering SNR increases the ambient noise levels, and therefore, the convergence effect around the critical window length is reduced in Figs. 17 and 24. However, the convergence effect is still seen in Fig. 24, for the channel in Fig. 20, which has significantly less lower-magnitude channel components from diffused reflection, and therefore, less vulnerable to low SNR issues.

The principal difference between the NMSE results for the two types of channels (Figs. 1 and 20) is that for the simulated channel (Fig. 20), NMSE decreases for increasing window length (refer to Figs. 23 and 24). This is because this channel has more slowly varying channel components due to relatively steady multipath arrivals from specular reflections. Therefore, for the simulated channel (Fig. 20) the slowly varying components occupying the lower Doppler frequencies, as seen in Fig. 21, dominate the 2D Fourier domain than the estimated channel in Fig. 1. Therefore, Figs. 23 and 24 exhibit an improvement in NMSE as the averaging window length increases whereas Figs. 16 and 17 show an optimal window length where NMSE is minimized before increasing again. It is noteworthy that for sufficiently long window lengths similar minima is expected for Figs. 23 and 24 as well, as the gain in high-precision estimation of the steady-state components is slowly offset by the loss in precision to capture the transient variations.

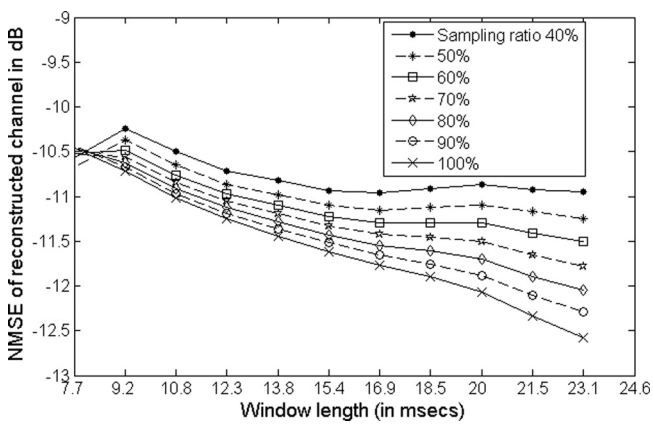

FIG. 24. NMSE results on channel estimation at 5 dB SNR with modified CS, support T is zero and first five non-zero Doppler frequencies; implements Eq. (15).

V. CONCLUSIONS

A 2D frequency domain representation is introduced that captures the time-varying fluctuations of the shallow water acoustic channel both in delay frequency and Doppler frequencies. The chief advantage of choosing this 2D frequency domain is that it disambiguates the slowly varying channel components which occupy the lower frequency bands, against the transient channel components, which are difficult to model or predict, and typically occupy the higher frequency bands. Furthermore, the transient channel components occupying the higher frequencies typically manifest a sparser distribution locally, than their slowly varying counterparts in the lower frequency bands. This disambiguation of diverse channel effects within the 2D spectra is exploited to introduce non-uniform compressive sampling, where different sampling ratios are employed at different frequency bands to take advantage of the relative sparsity of different types of channel components. This work is scoped to the channel estimation aspects with no feedback or iteration between transmitter and receiver. Proposed methods are validated through extensive numerical simulations. These numerical experiments employ two independent channels as the simulation setup: (i) field estimates from the SPACE08 experiment using established techniques, as well as (ii) a public-domain channel simulator that emulates well-known oceanic phenomena such as specular reflections, and have been tested against real channel estimates from field trials. Overall, the conclusion of these investigations shows consistent results between the two types of independent numerical experimentation. Simulation results demonstrate that the optimal operating point of channel observation is an intricate combination of observation window length, local sparsity of the channel support (e.g., within a given frequency band), as well as the sampling ratio appropriate for that local (and typically unknown in advance) sparsity. An adaptive technique is also provided that heuristically estimates the locally optimal operating point by minimizing the normalized prediction error for the estimated channel locally. Simulation results also demonstrate that while, as expected the NMSE improves with increasing sampling ratio, the performance gap between high and low sampling ratios is within 1 dB when operating around (or close to) this optimal operating point. This is well-known in compressive sampling, where the primary gain is achieving similar error rates using drastically smaller sampling ratios. This work articulates the same concept for shallow water acoustic communications, and introduces a non-uniform compressive sampling framework in a 2D frequency domain, that is cognizant of the fundamentally intertwined nature of the shallow water acoustic channel: between non-stationary transient elements, and relatively steady channel components due to diverse multipath phenomena.

ACKNOWLEDGMENTS

The authors would like to thank Dr. James Preisig, WHOI, for providing experimental field data collected at the SPACE08 experiment. The SPACE08 experiment was conducted by Dr. James Preisig, WHOI, and was supported by ONR Grant Nos. N000140710738, N000140510085, N000140710184, and N000140710523. N.A. would like to thank Council of Scientific & Industrial Research (CSIR), Government of India, for financial support.

APPENDIX

Below is the list of parameters used to simulate an UWA channel used in Sec. IV (refer to Fig. 20 generated using Ref. 4, with the help of MATLAB code present at Ref. 31).

$h0 = 103$; {surface height (depth) [m]}
$ht0 = 58$; (Transmitter height [m])
$hr0 = 59$; (Receiver height [m])
$d0 = 3000$; (channel distance [m])

$k = 1.7$; (spreading factor)
$c = 1500$; (speed of sound in water [m/s])
$c2 = 1200$; {speed of sound in bottom [m/s] (>1500 for hard, <1500 for soft)}
cut = 20; (do not consider arrivals whose strength is below that of direct arrival divided by cut)

$fmin = 8.5 \times 10^3$; (minimum frequency [Hz])
$B = 9 \times 10^3$; (bandwidth [Hz])

$df = 25$; (frequency resolution [Hz], $f\_vec = fmin{:}df{:}fmax$;)

$dt = 50 \times 10^{-3}$; (time resolution [seconds])
$T\_SS = 60$; (coherence time of the small-scale variations [seconds])

Small-Scale (S-S) parameters:
sig2s = 1.125; (variance of S-S surface variations)
sig2b = sig2s/2; (variance of S-S bottom variations)

$B\_delp = 5 \times 10^{-4}$; [3-dB width of the p.s.d. of intra-path delays (assumed constant for all paths)]
Sp = 20; [number of intra-paths (assumed constant for all paths)]
mu_p = 0.5/Sp; [mean of intra-path amplitudes (assumed constant for all paths)]
$nu\_p = 1 \times 10^{-6}$; [variance of intra-path amplitudes (assumed constant for all paths)]
Large-Scale (L-S) parameters:
T_tot = 3*T_SS; (total duration of the simulated signal [seconds])
t_tot_vec = (0:dt:T_tot); Lt_tot = length(t_tot_vec);

h_bnd = [−10 10]; [range of surface height variation (L-S realizations are limited to h + h_band)]
ht_bnd = [−5 5]; (range of transmitter height variation)
hr_bnd = [−5 5]; (range of receiver height variation)
d_bnd = [−20 20]; (range of channel distance variation)
sig_h = 1; (standard deviation of L-S variations of surface height)
sig_ht = 1; (standard deviation of L-S variations of transmitter height)
sig_hr = 1; (standard deviation of L-S variations of receiver height)
sig_d = 1; (standard deviation of L-S variations of distance height)

a_AR = 0.9; [AR parameter for generating L-S variations (constant for variables h, ht, hr, d)]

[1]W. Li and J. C. Preisig, "Estimation of rapidly time-varying sparse channels," IEEE J. Ocean. Eng. **32**(4), 927–939 (2007).
[2]E. V. Zorita and M. Stojanovic, "Space-frequency block coding for underwater acoustic communications," IEEE J. Ocean. Eng. **40**(2), 303–314 (2015).
[3]A. Radosevic, R. Ahmed, T. M. Duman, J. G. Proakis, and M. Stojanovic, "Adaptive OFDM modulation for underwater acoustic communications: Design considerations and experimental results," IEEE J. Ocean. Eng. **39**(2), 357–370 (2014).
[4]P. Qarabaqi and M. Stojanovic, "Statistical characterization and computationally efficient modeling of a class of underwater acoustic communication channels," IEEE J. Ocean. Eng. **38**(4), 701–717 (2013).
[5]Y. M. Aval and M. Stojanovic, "Differentially coherent multichannel detection of acoustic OFDM signals," IEEE J. Ocean. Eng. **40**(2), 251–268 (2015).
[6]B. Li, S. Zhou, M. Stojanovic, L. Freitag, and P. Willett, "Multicarrier communication over underwater acoustic channels with nonuniform Doppler shifts," IEEE J. Ocean. Eng. **33**(2), 198–209 (2008).
[7]E. Calvo and M. Stojanovic, "Efficient channel-estimation-based multiuser detection for underwater CDMA systems," IEEE J. Ocean. Eng. **33**(4), 502–512 (2008).
[8]A. Sen Gupta and J. Preisig, "A geometric mixed norm approach to shallow water acoustic channel estimation and tracking," Phys. Commun. **5**(2), 119–128 (2012).
[9]M. Chitre, "A high-frequency warm shallow water acoustic communications channel model and measurements," J. Acoust. Soc. Am. **122**(5), 2580–2586 (2007).
[10]P. Bello, "Characterization of randomly time-variant linear channels," IEEE Trans. Commun. Syst. **11**(4), 360–393 (1963).
[11]A. Sen Gupta, "Time-frequency localization issues in the context of sparse process modeling," Proc. Meet. Acoust. **19**, 070084 (2013).
[12]J. C. Preisig and G. B. Deane, "Surface wave focusing and acoustic communications in the surf zone," J. Acoust. Soc. Am. **116**(4), 2067–2080 (2004).
[13]B. Tomasi, J. Preisig, G. B. Deane, and M. Zorzi, "A study on the wide-sense stationarity of the underwater acoustic channel for non-coherent communication systems," in *11th European Wireless Conference 2011-Sustainable Wireless Technologies* (*European Wireless*), Vienna, Austria (2011), pp. 1–6.
[14]A. Sen Gupta and J. Preisig, "Tracking the time-varying sparsity of channel coefficients in shallow water acoustic communications," in *IEEE 2010 Conference Record of the Forty Fourth Asilomar Conference on Signals, Systems and Computers (ASILOMAR)* (2010), pp. 1047–1049.
[15]A. Sen Gupta and J. Preisig, "Adaptive sparse optimization for coherent and quasi-stationary problems using context-based constraints," in *IEEE International Conference on Acoustics, Speech and Signal Processing (ICASSP)* (2012), pp. 3413–3416.
[16]S. F. Cotter and B. D. Rao, "Sparse channel estimation via matching pursuit with application to equalization," IEEE Trans. Commun. **50**(3), 374–377 (2002).
[17]C. R. Berger, S. Zhou, J. C. Preisig, and P. Willett, "Sparse channel estimation for multicarrier underwater acoustic communication: From subspace methods to compressed sensing," IEEE Trans. Signal Process. **58**(3), 1708–1721 (2010).
[18]J. Huang, C. R. Berger, S. Zhou, and P. Willett, "Iterative sparse channel estimation and decoding for underwater MIMO-OFDM," EURASIP J. Adv. Signal Process. **2010**(1), 1 (2010).
[19]K. Pelekanakis and M. Chitre, "New sparse adaptive algorithms based on the natural gradient and the-norm," IEEE J. Ocean. Eng. **38**(2), 323–332 (2013).
[20]P. Ceballos Carrascosa and M. Stojanovic, "Adaptive channel estimation and data detection for underwater acoustic MIMO-OFDM systems," IEEE J. Ocean. Eng. **35**(3), 635–646 (2010).
[21]E. J. Candes, J. K. Romberg, and T. Tao, "Stable signal recovery from incomplete and inaccurate measurements," Commun. Pure Appl. Math. **59**(8), 1207–1223 (2006).
[22]J. A. Tropp and A. C. Gilbert, "Signal recovery from random measurements via orthogonal matching pursuit," IEEE Trans. Inf. Theory **53**(12), 4655–4666 (2007).
[23]D. Needell and J. A. Tropp, "CoSaMP: Iterative signal recovery from incomplete and inaccurate samples," Appl. Comput. Harmonic Anal. **26**(3), 301–321 (2009).
[24]S. S. Haykin, *Adaptive Filter Theory* (Pearson Education, India, 2008), pp. 1–921.
[25]R. Tibshirani, "Regression shrinkage and selection via the lasso," J. R. Soc. Stat. Soc. B **58**, 267–288 (1996).
[26]D. L. Donoho, "Compressed sensing," IEEE Trans. Inf. Theory **52**(4), 1289–1306 (2006).
[27]E. J. Candès, "The restricted isometry property and its implications for compressed sensing," C. R. Mathematique **346**(9), 589–592 (2008).
[28]D. L. Donoho, "For most large underdetermined systems of linear equations the minimal l_1-norm solution is also the sparsest solution," Commun. Pure Appl. Math. **59**(6), 797–829 (2006).
[29]E. J. Candes and Y. Plan, "A probabilistic and RIPless theory of compressed sensing," IEEE Trans. Inf. Theory **57**(11), 7235–7254 (2011).
[30]N. Vaswani and W. Lu, "Modified-CS: Modifying compressive sensing for problems with partially known support," IEEE Trans. Signal Process. **58**(9), 4595–4607 (2010).
[31]P. Qarabaqi and M. Stojanovic, "Acoustic channel modeling and simulation" (2013). http://millitsa.coe.neu.edu/?q=projects (Last viewed 10 November 2016).
[32]R. Nadakuditi and J. C. Preisig, "A channel subspace post-filtering approach to adaptive least-squares estimation," IEEE Trans. Signal Process. **52**(7), 1901–1914 (2004).
[33]M. Lustig, D. L. Donoho, J. M. Santos, and J. M. Pauly, "Compressed sensing MRI," IEEE Signal Process. Mag. **25**(2), 72–82 (2008).
[34]M. Lustig, D. L. Donoho, and J. M. Pauly, "Sparse MRI: The application of compressed sensing for rapid MR imaging," Magnetic Resonance Med. **58**(6), 1182–1195 (2007).
[35]E. Van den Berg and M. P. Friedlander, "Sparse optimization with least-squares constraints," SIAM J. Optimization **21**(4), 1201–1229 (2011).
[36]E. van den Berg and M. P. Friedlander, "Probing the Pareto frontier for basis pursuit solutions," SIAM J. Sci. Comput. **31**(2), 890–912 (2008).
[37]E. van den Berg and M. P. Friedlander, "SPGL1: A solver for large-scale sparse reconstruction," June 2007. http://www.cs.ubc.ca/labs/scl/spgl1 (Last viewed 10 November 2016).
[38]J. Romberg, "Imaging via compressive sampling [introduction to compressive sampling and recovery via convex programming]," IEEE Signal Process. Mag. **25**(2), 14–20 (2008).
[39]E. J. Candès, J. Romberg, and T. Tao, "Robust uncertainty principles: Exact signal reconstruction from highly incomplete frequency information," IEEE Trans. Inf. Theory **52**(2), 489–509 (2006).
[40]A. Sen Gupta, N. Ansari, and A. Gupta, "Tracking the underwater acoustic channel using two-dimensional frequency sampling," in *IEEE OES International Symposium on Underwater Technology*, Chennai, India (2015), pp. 1–5.
[41]N. Ansari, A. Gupta, and A. Sen Gupta, "Physics inspired CS based underwater acoustic channel estimation," in *IEEE Global Conference on Signal and Information Processing (GlobalSIP)* (2015), pp. 1106–1110.